Coronal lines and the importance of deep-core–valence correlation in Ag-like ions

Jon Grumer,[1,*] Ruifeng Zhao,[2,3] Tomas Brage,[1] Wenxian Li,[2,3] Sven Huldt,[4] Roger Hutton,[2,3] and Yaming Zou[2,3]
[1]*Division of Mathematical Physics, Department of Physics, Lund University, Sweden*
[2]*The Key Laboratory of Applied Ion Beam Physics, Ministry of Education, China*
[3]*Shanghai EBIT Laboratory, Modern Physics Institute, Fudan University, Shanghai, China*
[4]*Lund Observatory, Lund University, Sweden*
(Received 12 May 2014; published 30 June 2014)

We report on large-scale and critically evaluated *ab initio* multiconfiguration Dirac-Hartree-Fock calculations of the wavelength and transition rate of the "coronal," $M1$ transition $4f\ ^2F^o_{5/2}$–$^2F^o_{7/2}$ in Ag-like ions. The transition between these two fine-structure levels, which makes up the ground term for $Z \geqslant 62$ in the isoelectronic sequence, has recently been observed in Yb^{23+} and W^{27+}, where the latter could be of great importance for fusion plasma diagnostics. We present values for all members of the sequence between $Z = 50$ and 94, which are supported by excellent agreement with values from recent experiments. The importance of including core-valence correlation with the $n = 3$ shell in the theoretical model is emphasized. The results show close-to-spectroscopic accuracy for these forbidden lines.

DOI: 10.1103/PhysRevA.89.062511 PACS number(s): 31.15.A−, 31.15.V−, 32.70.Cs

I. INTRODUCTION

Forbidden magnetic-dipole ($M1$) transitions take place between states of the same parity. In particular, such transitions among ground-state levels in highly charged ions can be in the visible spectral region and have quite low transition rates. The most famous $M1$ transitions are the so-called *coronal lines*, whose origin was unknown for more than 70 years before Edlén identified several of them as ground state $M1$ lines in 9- to 15-times ionized ions, mainly Ca, Fe, and Ni, in 1942 [1,2]. Not for many years would it be possible to observe such lines in laboratory light sources. In 1978 Suckewer and Hinnov [3] made the first observation of an $M1$ transition in a fusion plasma. From the Doppler width of this line, 2665 Å in Fe XX, a record temperature (at that time) of 45×10^6 K was derived for the Princeton Large Torus tokamak. In tokamaks, the solar corona, and in particular electron beam ion traps (EBITs), the plasma density is low enough for such lines to appear. In other terrestrial light sources for highly charged ions, e.g., sparks and laser produced plasmas, the long radiative lifetimes of the excited levels responsible for $M1$ transitions would lead to collisional quenching. It is interesting to note that Edlén could not observe the $M1$ lines he identified in the solar corona using contemporary laboratory light sources due to density problems. His identifications were based on his established energy levels from soft x-ray spectroscopy. In the same way an attempt to establish the energy difference between the Ag-like ground state $4d^{10}\,4f\ ^2F_{5/2}$ and $^2F^o_{7/2}$ levels (for $Z \geqslant 62$), which is the subject of the work presented here, was only done through soft x-ray spectroscopy [4].

We observed the actual $M1$ transition connecting these two levels on Ag-like W [5] and, recently, Yb [6]. The lifetime of the upper level being in the millisecond range places interesting requirements on the density of the light source. EBITs with electron densities on the order of 1012 cm^{-3}, or less, are ideal light sources for studying such transitions. Although the electron density in EBITs is lower than tokamak fusion plasma densities, by around 2 orders of magnitude, $M1$ lines have been observed in fusion devices, e.g., as mentioned above the $2s^2\,2p^3\ ^2D_{5/2}$–$^2D_{3/2}$ $M1$ decay in Fe XX [3]. Also, at the National Institute for Fusion Science in Japan, Morita *et al.* [7] reported the observation of $M1$ transitions in the visible region for highly charged tungsten ions. Previously spectra from tokamaks made a great impact on the study of $M1$ and other forbidden transitions (see Ref. [8] for details). With EBITs it is possible to measure both wavelengths and lifetimes of $M1$ [9] and even higher-order transitions in highly charged ions, for example, the studies of the $M3$ decay in Ni-like Xe [10] and later Ni-like W [11].

$M1$ transitions in highly charged ions with seemingly simple ground states such as the Ag-like $4d^{10}\,4f\ ^2F^o_{5/2,7/2}$ doublet are interesting testing grounds for theoretical methods since (a) for some ions along a sequence the $M1$ line will be a visible transition and therefore accessible to accurate measurement and (b) the calculation could be sensitive to correlation from deeper bound electrons, first noted in Ref. [5] and further investigated in this work. Finally, (c) it is also possible that the results could be useful as a test of quantum-electrodynamical effects.

In the present work we use a systematic approach to calculate the wavelength of these $M1$ transitions in Ag-like ions. The $4d^{10}\,4f\ ^2F$ is the ground term for ions with $Z > 61$, while at the neutral end the $4d^{10}\,5s^2S$ forms the ground state. Adopting the multiconfiguration Dirac-Hartree-Fock (MCDHF) approach, we carefully monitor the accuracy of the transition energy within different electron correlation models as a function of basis size. To further support the identification of these $M1$ lines, we use an isoelectronic analysis. The agreement between theory and experiment should be consistent for several ions and the trend of different atomic properties ought to behave smoothly as a function of the nuclear charge along the sequence.

Some previous isoelectronic work has been reported for theoretical work on Ag-like systems. Safronova *et al.* [12] used the relativistic many-body perturbation theory (RMBPT) to study the energies of the singly excited states $4d^{10}\{4f, 5s, 5p, 5d, 5f, 5g\}$ for ions between $Z = 48$ and

*jon.grumer@teorfys.lu.se

100. The energy structures were unfortunately only tabulated for a few selected ions at the neutral end, but the rest was made available through the more recent publication of binding energies by Ivanova [13], from which it is possible to extract the $4f\,^2F^o$ fine-structure energy separations. Comparison with these results along the sequence provides a reliable benchmark for the present study, especially due to the different nature, perturbative versus variational, of the two methods. Ivanova also reported a few years earlier on calculations of Ag-like ions with $Z = 52$ to 86 based on relativistic perturbation theory with a model potential (RPTMP) [14]. Finally, there is a recent, but more limited in terms of correlation, MCDHF calculation by Ding *et al.* [15].

The aim of the present work is to use systematic isoelectronical analysis of electron correlation to provide solid support to the experimental identifications of the $4d^{10}\,4f\,^2F^o_{5/2}$–$^2F^o_{7/2}$ $M1$ transition in Ag-like W [5] and Yb [6] as well as future measurements in the mid- and, especially, high-Z range of the sequence. These new data should also, in addition to constituting a theoretical benchmark, be useful to the astrophysical- and fusion-plasma community.

II. METHOD OF CALCULATION

The $4f\,^2F^o_{5/2,7/2}$ atomic wave functions are determined along the Ag I sequence using the MCDHF method in the form of the most recently published version of the well-established fully relativistic GRASP2K code [16], originally developed by Grant and coworkers [17,18].

A. Basic multiconfiguration Dirac-Hartree-Fock theory

The MCDHF method is outlined in detail in Grant's book [19] and the nonrelativistic variant of the approach is covered by Froese Fischer *et al.* [20]. Here we will only discuss the basic, and for our work most important, concepts.

The starting point for the MCDHF theory is to define an atomic state function, $|\Gamma J^\pi\rangle$, as a linear combination of configuration state functions (CSFs), $|\gamma_i J^\pi\rangle$,

$$|\Gamma J^\pi\rangle = \sum_i c_i\,|\gamma_i J^\pi\rangle\,, \tag{1}$$

where γ_i are labels to uniquely define the CSFs and c_i are expansion coefficients. The Γ is usually chosen as the γ_i of the CSF with maximum weight c_i^2. The CSFs are, in turn, anti-symmetrized products of single-electron Dirac orbitals coupled to eigenfunctions of the total angular momentum (J^2 and J_z) and parity (π) operators. Without going into any details the MCDHF approach is essentially a multireference self-consistent field method based on the many-body Dirac-Coulomb Hamiltonian, expressed as

$$\mathcal{H}_{\rm DC} = \sum_i^N h_D(\boldsymbol{r}_i) + \sum_{i>j}^N 1/r_{ij}, \tag{2}$$

in Hartree atomic units. Here h_D is the standard one-particle Dirac Hamiltonian and the second sum represents the instantaneous, interelectronic Coulomb interaction.

The CSF basis expansion is generated in an active space (AS) approach in which a limited number of Dirac orbitals are divided into an inactive and active set. The CSF expansion is then formed through single (S), double (D), triple (T), etc., substitutions from a set of predefined important CSFs, the multireference (MR) set, to the active set of orbitals. A calculation on the MR set builds the zero order wave function. Orbitals of closed shells in the MR set are typically defined as inactive and therefore not a part of the active set.

The set of Dirac orbitals and mixing coefficients are optimized to self-consistency in the MCDHF procedure, followed by a relativistic configuration interaction calculation in order to include the Breit interaction and leading QED effects. The Breit interaction is evaluated in the low-frequency limit of the exchanged virtual photon. The contribution from vacuum polarization is included to second- (Uehling) and fourth-order (Källén-Sabry) [21]) and the self-energy is evaluated in the hydrogenic approximation with reference values from Ref. [22]).

The computational accuracy is essentially determined by whether the necessarily finite set of CSFs is effectively complete for the atomic states under investigation. This is dependent on the choice of included CSFs but also on the optimization of and constraints on the Dirac orbitals. In practice the accuracy of the method is evaluated through careful convergence studies of atomic properties as a function of different correlation models and CSF expansions within these models. The latter is defined by the size of the active set of correlation orbitals. In GRASP2K the calculations are performed in a layer-by-layer scheme, in which the AS of CSFs is enlarged systematically. The orbitals belonging to previous layers, defined by, e.g., their principal quantum number n, are kept fixed in the variational procedure and only the new ones are optimized.

B. Correlation models

Two different computational models are presented in this work. The first (separate core-valence) is designed to provide information about important correlation contributions. Based on the experience gained from this calculation it is possible to design a large-scale model (full core-valence) with the goal of reaching high-enough accuracy for what we could label as *single-line spectroscopy*.

Both models use $[1s^2\,2s^2\ldots4d^{10}\,4f]^o_{5/2,7/2}$ as the MR set, i.e., two separate CSFs build the $J = 5/2$ and $7/2$ symmetry blocks. These CSFs are constructed from a common set of orbitals, optimized on a linear combination of the energies of the lowest state of each block (extended optimal level). In this work the Dirac-Fock (DF) method is defined as the case when the CSF expansion only includes the MR set. The orbitals obtained in the initial DF step are then kept frozen throughout the remaining procedure. To include correlation, the basis set is enlarged through substitutions from this reference configuration to a systematically increased set of CSFs.

1. A separate core-valence correlation model

In order to obtain an *ab initio* transition energy of close to spectroscopic accuracy, we need a detailed investigation of the correlation between valence and core electrons, or core-valence (CV) correlation. In the MCDHF scheme, CV correlation is represented by CSFs obtained from simultaneous

replacements of one core and one valence electron of the CSFs in the MR set, with those in the active set of orbitals. In the special case of a singly occupied valence subshell, such as in the $4f$ configuration of Ag-like ions, the inclusion of CV correlation will in general increase the binding energy of this electron as compared to a fixed core calculation. The orbital of the single valence electron will therefore in many cases be contracted, which might have a large impact on different atomic properties.

CV correlation is often thought of as the MCDHF representation of core polarization. This is, however, a too-simplistic interpretation. CV correlation does in general also include radial correlation through CSFs which only differ in the principal quantum number n from the reference CSFs. It is also clear that true core polarization should be evaluated by comparisons with results using core orbitals optimized on the bare core only, as the $4f$-electron polarizes the core, and not with the DF results of the $|\ldots 4d^{10}\,4f\,{}^2F^o\rangle$ states as we do here. We will therefore refer to core-valence correlation rather than core polarization.

Turning to the $4d^{10}\,4f$ states of Ag-like ions, it was recently shown for Ag-like W [5] that a major part of the contribution from core-valence correlation to the fine-structure separation $4f\,{}^2F^o_{5/2,7/2}$ is due to interaction with the $3d$ subshell. This is maybe counterintuitive as one would expect that the largest contributions should come from the outermost core subshells, i.e., $4d$ in this case. We will investigate this further along the Ag-like sequence.

Defining the singly occupied $4f$ subshell as the only valence shell implies that there is no valence-valence (VV) correlation. This allows for separate studies of the energy contributions from interactions between the valence electron and the different core subshells, one subshell at a time. Such as separate core-valence (SCV) study should provide valuable information about electron correlation, usable when designing a large-scale model including possible "interference" effects between contributions from different core subshells.

To be more specific, the SCV calculations proceed with separate calculations for each subshell contribution, including only CSFs with one hole in a distinct core subshell. As an example, if we include only CSFs of the form $1s^2\,2s^2\ldots 3p^5\ldots 4d^{10}\,nl\,n'l'$, where an electron from the $3p$ core subshell is allowed to be excited together with the $4f$ valence electron, we include CV correlation with $3p$. We aim in each calculation for converged results of the ^2F energy separation, as a function of the maximum n and l of the orbitals included in the active set. Taking the difference of the converged and the DF energy separation gives an estimate of the energy contribution due to CV correlation with the chosen core subshell ($3p$ in our example). Adding all these SCV contributions to the DF energy value, gives an estimate of the total fine-structure separation. It should be clear that this approach only is applicable to systems with a single valence electron since it otherwise is impossible to separate the VV and CV contributions.

2. Full core-valence correlation model

With the results from the SCV model at hand, it is feasible to design a large-scale model in which CV correlation with all subshells (except $1s$) is included simultaneously in the MCDHF procedure. This will be referred to as the full core-valence (FCV) model.

This model contains CSFs generated from simultaneous substitutions of at most one electron from any subshell down to $n = 2$, together with the $4f$ valence electron of the reference configuration to the active set of orbitals. The $1s$ subshell is kept closed as it proved having a negligible effect on the $^2F^o$ energy separation. Furthermore, the CSFs of the $4d^8\,4f^3$ configuration (the most important CSFs in the $n = 4$ complex in addition to $4d^{10}\,4f$) are also added. The orbital set is increased up to $n = 10$ and $l = 6$ (i orbitals), which corresponds to a maximum of 39 230 CFSs in the $J = 5/2$ block and 43 857 CSFs in the $J = 7/2$ block. These seem to be quite reasonably sized basis sets at first glance, but the calculation still takes a few weeks to run per charge state (with the serial version of the codes on modern 3.7-GHz Intel Xeon-based computers) due to comparatively dense energy matrices.

III. RESULTS AND DISCUSSION

We start this section with a discussion of the experiences gained from the smaller SCV model. This is followed by results from the large-scale FCV calculation, together with comparisons with other recent theoretical and experimental results. There is a special focus on the differences in the amount of core-valence correlation included in the different models and the impact of this on the final fine-structure separations for different members of the isoelectronic sequence. In the final section we present rates for the magnetic-dipole transitions.

A. The impact of core-valence correlation

The SCV calculation reveals interesting trends of the effect of core-valence correlation on the fine-structure separation along the isoelectronic sequence as can be seen in Fig. 1. In this plot the energy contribution due to CV correlation with all core subshells down to $2s$ is presented for ions between $Z = 50$ and 92. For the ions at the neutral end it is clear that the CV contribution from $4d$ is large as would be expected. However, for $Z \geqslant 58$ the major contribution is due to $3d$ and it becomes increasingly dominant as Z increases, followed by CV correlation with $3p$ and $4p$. For $Z = 94$ the correlation with $3d$ makes up 46% of the total contribution. It is also interesting to note that the impact of correlation with $4d$ becomes almost negligible for $Z \geqslant 70$ and actually gives a negative contribution for $70 < Z < 85$. The fact that CV correlation with deeper core shells becomes an important factor in the calculation of this fine-structure separation was first noted for Ag-like W ($Z = 74$) [5], where correlation with $3d$ contributes with 51% of the total value and the whole $n = 3$ shell 78%.

Judging from the results of this initial investigation, one can conclude that core-valence correlation with essentially all core subshells is of importance to the fine-structure separation when aiming for high accuracy. In the low-Z regime it is clear that interactions with the $n = 4$ subshells are crucial, replaced by $3p$ and foremost $3d$ for higher members of the sequence.

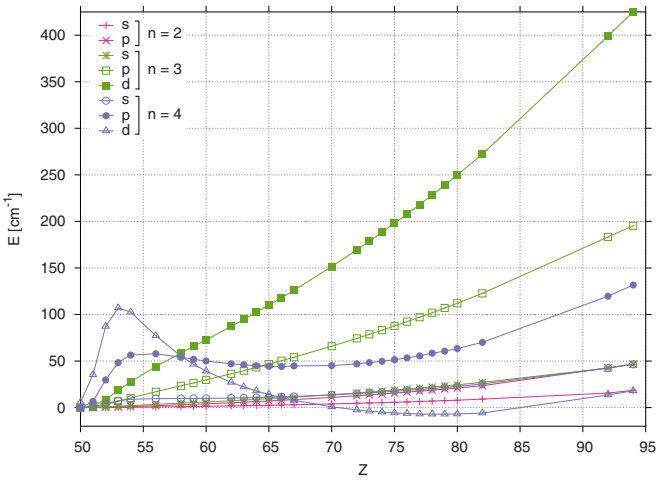

FIG. 1. (Color online) Absolute contributions from core-valence correlation with different core subshells relative to Dirac-Fock energies [$E = E_{\rm tot}^{\rm SCV}(nl) - E_{\rm DF}$, the SCV model is explained in the text] to the $4f\,^2F^o$ fine-structure energy separation of Ag-like ions with nuclear charges $50 \leqslant Z \leqslant 94$. This clearly shows the dominating behavior of core-valence correlation with $3d$ rather than $4d$ in the mid- and high-Z regime. Note that these energy contributions are presented as absolute numbers and not as a fraction of the total fine-structure energy separation, compared with Table I or Fig. 3 where the total energies are given.

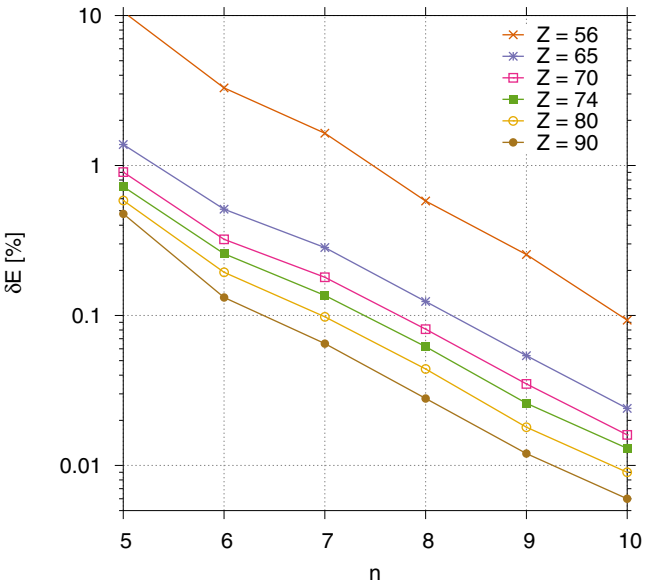

FIG. 2. (Color online) Relative convergence of the $^2F^o$ energy separation as the size of the active set of orbitals is increased in a layer-by-layer scheme, denoted by the principal quantum number n. δE is the difference in percentages of energy from the previous correlation layer.

B. The $4f\,^2F^o$ fine-structure separation from the FCV model

In this section we present results from $^2F^o$ energy separations along the Ag-like isoelectronic sequence from the large-scale FCV model in which core-valence correlation is included with all subshells except $1s$. The model has been carefully evaluated in terms of convergence of the energy separation of $^2F^o$ with respect to the size of the active set of Dirac orbitals. Within the boundaries of this model it can be seen from Fig. 2, which shows the convergence trend (difference in energy from previous correlation layer as a fraction of the total fine structure) in a logarithmic scale, that the fine-structure separation has been converged to close to 0.1% for $Z = 56$ and to 0.006% for $Z = 90$.

Resulting energies for all ions in the Ag-like isoelectronic sequence with nuclear charges $50 \leqslant Z \leqslant 94$ are presented in Table I and Fig. 3. In the second column we give the Dirac-Fock energies from the MCDHF (Dirac-Coulomb) approach, where a negative value corresponds to an inverted fine structure. The third column contains energy contributions due to the frequency-independent Breit interaction, and the fourth shows leading QED effects. The impact of electron correlation in the regime of the Dirac-Coulomb-Breit-QED Hamiltonian (calculated by taking the difference of the DF and the converged FCV results) is presented in the fifth column. Finally, the sixth column and Fig. 3 give the total energy separation, including all the above-mentioned contributions. It is clear that correlation is the dominating correction to DF (Dirac-Coulomb) in the low-Z regime, replaced by the Breit interaction for $Z \geqslant 57$. The energy shift due to the QED corrections are comparatively small along the whole sequence.

C. Comparison with experiment and other theory

The fine-structure energy separations from experimental and other theoretical results are compared to our FCV values in Table II and plotted as differences to our FCV results in Fig. 4. As shown in Fig. 3, the trend of the fine-structure splitting along the sequence should be smooth, in the absence of level crossings or other effects. We should therefore expect a similar behavior for other methods and thereby also for the difference between different sets of results.

The agreement of our results with most of the experimental data points is in general very good, with the largest deviations between $Z = 62$ and 66, where the $4d^{10}\,4f\,^2F^o$ term becomes the ground state ($Z = 62$). The experimental values do, however, show an irregular isoelectronic trend for low-Z ions, which warrant further investigations. For higher nuclear charges there is an excellent agreement (less than 0.1%) with the two most recent experimental results: 19 383 cm^{-1} for Yb ($Z = 70$) [6] and 29 600 cm^{-1} for W ($Z = 74$) [5].

There is also a good agreement between our results and the RMBPT calculation, especially in the beginning and at the high end of the sequence. More importantly, in the two ends, the difference between the two data sets behaves in smooth way, except for the leap between $Z = 57$ and 61. It is important to note, however, that the RMBPT values are collected from two sets of data, presented in two different publications ($Z \leqslant 57$ from Safronova *et al.* [12] and $Z \geqslant 61$ from Ivanova [13]). The leap in energy might therefore be due to some inconsistency between the two papers or in the model. Another possibility is close degeneracy caused by level crossings as the $4f$ configuration becomes the ground state, which could be difficult to represent in a perturbative approach.

The difference between our results and the earlier MCDHF calculation [15] is most likely explained by their exclusion of

TABLE I. The fine-structure separation of $4f\ ^2F^o_{5/2,7/2}$ from the FCV calculation (see text for details). The first column shows the atomic number, Z and the second ($E^{\rm DC}_{\rm DF}$) gives the energy separations resulting from single-CSF calculations, here referred to as Dirac-Fock (DF), based on the DC Hamiltonian. The third column (δE_B) presents additional energy contributions due to the Breit interaction in the low-frequency limit (B). The fourth ($\delta E_{\rm QED}$) presents the total contribution from self-energy and vacuum polarization (QED) corrections. The fifth column ($\delta E_{\rm corr}$) shows how big the influence of correlation is in the DC + B + QED scheme. In the sixth column ($E_{\rm tot}$) the total energy separations (including Breit, QED and correlation) are presented. All energies are given in cm^{-1} and a negative total energy value corresponds to an inverted fine structure (i.e., the $J = 7/2$ level having lowest energy).

Z	$E^{\rm DC}_{\rm DF}$	$+\delta E_B$	$+\delta E_{\rm QED}$	$+\delta E_{\rm corr}$	$=E_{\rm tot}$
50	−88	−3	0	6	−85
51	−182	−13	0	59	−136
52	−161	−37	0	157	−41
53	62	−70	0	213	205
54	441	−106	0	229	564
55	925	−145	1	229	1010
56	1495	−186	1	225	1535
57	2145	−229	1	221	2139
58	2877	−274	2	218	2823
59	3696	−323	2	217	3592
60	4606	−374	3	217	4451
61	5613	−429	3	219	5406
62	6724	−488	4	223	6463
63	7946	−550	5	227	7628
64	9286	−616	5	234	8909
65	10 749	−686	6	241	10 311
66	12 344	−760	8	250	11 842
67	14 078	−838	9	260	13 509
68	15 958	−920	10	271	15 320
69	17 992	−1006	12	283	17 280
70	20 188	−1098	13	295	19 399
71	22 554	−1193	15	310	21 685
72	25 097	−1294	17	325	24 145
73	27 826	−1400	20	341	26 786
74	30 750	−1510	22	358	29 619
75	33 876	−1626	25	376	32 651
76	37 215	−1747	27	394	35 890
77	40 774	−1873	31	414	39 346
78	44 564	−2005	34	436	43 028
79	48 592	−2143	37	458	46 945
80	52 869	−2286	41	481	51 106
81	57 405	−2435	45	506	55 521
82	62 209	−2590	50	531	60 199
83	67 290	−2752	55	557	65 151
84	72 660	−2919	60	585	70 385
85	78 329	−3093	65	613	75 914
86	84 307	−3274	71	643	81 747
87	90 604	−3461	77	674	87 894
88	97 232	−3656	84	706	94 366
89	1 04 201	−3857	91	740	1 01 175
90	1 11 524	−4065	98	774	1 08 331
91	1 19 210	−4280	106	810	1 15 845
92	1 27 272	−4503	114	847	1 23 729
93	1 35 721	−4734	122	886	1 31 995
94	1 44 569	−4972	132	925	1 40 654

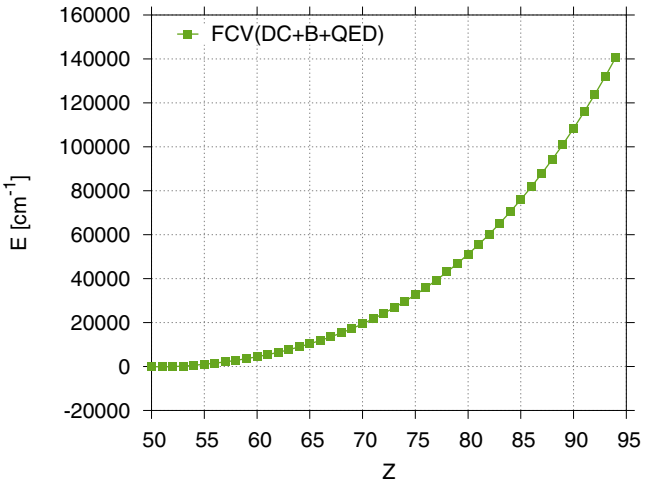

FIG. 3. (Color online) Energies of the $4d^{10}\,4f\ ^2F^o$ fine-structure separation from our FCV calculation along the Ag-like isoelectronic sequence.

core-valence correlation with other subshells than $4d$. From the earlier discussion about the SCV investigation (see Fig. 1) it was made clear the $n = 3$ shell contributes around 78% of the total amount of core-valence correlation, whereas the $4d$ subshell barely contributes at all for this Z. It is, however, hard to understand the irregular isoelectronic behavior of their results.

Finally, it is clear that there is a large inconsistency between the RPTMP results [14] and all other methods presented here, since the isoelectronic trend deviates from those predicted by others and shows inexplicable leaps.

To analyze the different theoretical methods and experiments further, we plot the contribution to the fine-structure separation due to electron correlation in Fig. 5. This is defined as the best available value (theoretical or experimental) from which the Dirac-Fock value is been subtracted. This again reveals a good agreement between our results and experiment, in terms of the individual data points and in the isoelectronic trend. The RMBPT results also agree well with both our results and the experimental values. Comparing this plot with Fig. 4 one can conclude that the earlier MCDHF [15] calculation lacks a major bulk of electron correlation necessary to reach a fine-structure separation close to experimental results. The irregular trend along the sequence mentioned above, especially the dip in energy around $Z = 65$, remains unexplained.

D. Magnetic-dipole transition probabilities

The calculation of the magnetic-dipole ($M1$) transition rate is almost trivial once the correct transition energy has been found, since the $M1$ operator is independent of the radial part of the wave function. In Table III the (vacuum) wavelength of the transition is presented along the isoelectronic sequence, together with the corresponding rates, weighted oscillator strengths, and line strengths. The simplicity of the $M1$ transition rate is reflected in the almost constant behavior of the line strength (which is independent of the transition energy). The small decrease seen with increasing Z is due to the CSF composition of the wave functions of the involved states via

TABLE II. Comparison of the $4f\,^2F^o_{5/2,7/2}$ energy separation obtained from the large-scale FCV model ($E^{\rm FCV}_{\rm tot}$) with experiment ($E_{\rm exp}$) (corresponding source(s) are given in the fourth column), and other available theory ($E_{\rm RMBPT}$ [12], $E_{\rm MCDHF}$ [15], and $E_{\rm RPTMP}$ [13,14]). All energies are given in $\rm cm^{-1}$ and the differences are presented relative to the FCV values of this work in absolute numbers δ_E and in percentages $\delta_{\%}$.

Z	$E^{\rm FCV}_{\rm tot}$	$E_{\rm exp}$	Source	δ_E	$\delta_{\%}$	$E_{\rm RMBPT}$	δ_E	$\delta_{\%}$	$E_{\rm MCDHF}$	δ_E	$\delta_{\%}$	$E_{\rm RPTMP}$	δ_E	$\delta_{\%}$
50	−85	−60	[23,24]	−24	40%	−76	−9	12%	−71	−14	20%			
51	−136					−162[b]	26	−16%	−121	−15	12%			
52	−41								−118	77	−66%			
53	205	200	[25]	5	2.7%	184	21	12%	71	134	189%			
54	564	550	[24,26]	14	2.5%	542	22	4.0%	411	153	37%			
55	1010	987	[24,27]	23	2.3%				854	156	18%			
56	1535	1516	[24,28]	19	1.3%				1380	155	11%			
57	2139	2160	[25]	−21	−1.0%	2123	16	0.7%	1984	155	7.8%			
58	2823	2784	[29]	39	1.4 %	2810	13	0.4%	2672	151	5.6%			
59	3592	3577	[29]	15	0.4 %				3442	150	4.3%			
60	4451	4430	[29]	21	0.5 %				4302	149	3.5%			
61	5406					5476[c]	−70	−1.3%	5253	153	2.9%	5272	134	2.5%
62	6463	6555	[29]	−92	−1.4%	6533[c]	−70	−1.1%	6301	162	2.6%	6353	110	1.7%
63	7628	7521 ± 62	[29]	107	1.4%	7697[c]	−69	−0.9%	7444	184	2.5%	7504	124	1.7%
64	8909	8900	[29][a]	9		8977[c]	−68	−0.8%	8685	224	2.6%	8800	109	1.2%
65	10 311	10 280	[29]	31	0.3%	10 378[c]	−67	−0.6%	10 033	278	2.8%	10 225	86	0.8%
66	11 842	11 770 ± 131	[29]	72	0.6%	11 908[c]	−66	−0.6%	11 512	330	2.9%	11 870	−28	0.2%
67	13 509	13 500	[29][a]	9	0.1%	13 573[c]	−64	−0.5%	13 140	369	2.8%	13 486	23	0.2%
68	15 320					15 383[c]	−63	−0.4%	14 926	394	2.6%	15 526	−206	−1.3%
69	17 280					17 341[c]	−61	−0.3%	16 871	409	2.4%	17 695	−415	−2.3%
70	19 399	19 383 ± 8	[6]	16	0.1%	19 459[c]	−60	−0.3%	18 979	420	2.2%	19 848	−449	−2.3%
71	21 685					21 741[c]	−56	−0.3%	21 254	431	2.0%	22 465	−780	−3.5%
72	24 145					24 198[c]	−53	−0.2%	23 702	443	1.9%	25 285	−1140	−4.5%
73	26 786					26 838[c]	−52	−0.2%	26 331	455	1.7%	28 350	−1564	−5.5%
74	29 619	29 600 ± 2	[5]	19	0.1%	29 668[c]	−49	−0.2%	29151	468	1.6%	31 769	−2150	−6.8%
75	32 651					32 696[c]	−45	−0.1%	32 167	484	1.5%	35 494	−2843	−8.0%
76	35 890					35 932[c]	−42	−0.1%	35 390	500	1.4%	39 491	−3601	−9.1%
77	39 346					39 385[c]	−39	−0.1%	38 828	518	1.3%	43 765	−4419	−10%
78	43 028					43 063[c]	−35	−0.1%	42 491	537	1.3%	48 320	−5292	−11%
79	46 945					46 976[c]	−31	−0.1%	46 387	558	1.2%	53 411	−6466	−12%
80	51 106					51 133[c]	−27	−0.1%	50 527	579	1.1%	58 754	−7648	−13%
81	55 521					55 542[c]	−21	0.0 %	54 918	603	1.1%	64 649	−9128	−14%
82	60 199					60 216[c]	−17	0.0 %	59 573	626	1.1%	70 791	−10 592	−15%
83	65 151					65 162[c]	−11	0.0 %	64 499	652	1.0%	77 338	−12 187	−16%
84	70 385					70 391[c]	−6	0.0 %	69 708	677	1.0%	84 066	−13 681	−16%
85	75 914					75 914[c]	0	0.0 %	75 209	705	0.9%	91 483	−15 569	−17%
86	81 747					81 741[c]	6	0.0 %	81 012	735	0.9%	99 145	−17 398	−18%
87	87 894								87 129	765	0.9%			
88	94 366								93 571	795	0.8%			
89	1 01 175								1 00 347	828	0.8%			
90	1 08 331								1 07 469	862	0.8%			
91	1 15 845								1 14 944	901	0.8%			
92	1 23 729								1 22 792	937	0.8%			
93	1 31 995													
94	1 40 654													

[a] based on interpolated values of $4f\,^2F^o_{7/2}$ [29].
[b] from Tab. 8 in Ref. [14].
[c] from Tab. 11 in Ref. [13].

interaction with other terms than $^2F^o$. This effect is, however, small since the ground term $^2F^o$ is well isolated in energy for most of the ions in the sequence.

Comparing these results with the transition rates presented in Table II of Ding *et al.* [15], it is clear that the rates from these two calculations differs substantially at the neutral end of the sequence. The discrepancy is especially profound for the few ions around $Z = 52$, which is not very surprising as this is where the fine-structure inversion takes place. The energy separations are small in this region of the sequence which

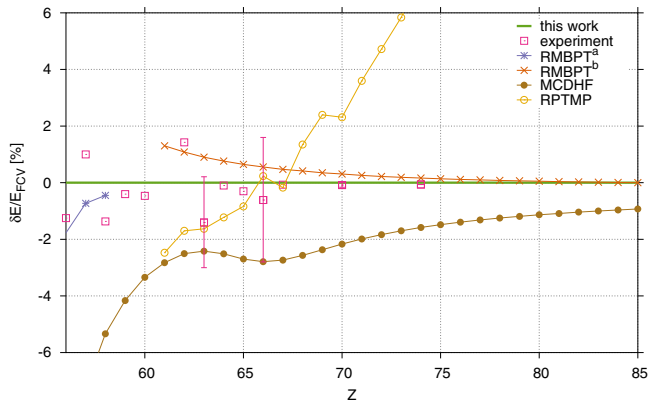

FIG. 4. (Color online) Experimental (see Table II for sources) and other theoretical (RMBPT[a] [12], RMBPT[b] [12] (from Ref. [13]), MCDHF [15], and RPTMP [13,14]) energies presented for an interesting subrange ($56 \geqslant Z \geqslant 85$) of the Ag-like isoelectronic sequence. The energy separations of the different sources are plotted as fractional differences relative to the FCV calculation $\delta E/E^{\rm tot}_{\rm FCV} = (E_{\rm method} - E^{\rm tot}_{\rm FCV})/E^{\rm tot}_{\rm FCV}$ in percentages. Error bars of four experimental data points were available and are included in the plot.

makes the $M1$ rate sensitive. For ions with $Z = 54$ to 59 the difference drops from 60 to 10% and continues to converge with increasing Z, reaching 5% for $Z = 74$ and 2% for $Z = 92$. The general trend that the results differ more for lower Z fits well with the above analysis that there are substantial electron correlation effects missing in the calculation by Ding *et al.*, which affects the ^2F separation and, hence, the $M1$ transition rate. It is therefore of interest to compare the transition-energy-independent line strength, S, which can be estimated from columns 2 (energy separation) and 3 (transition rate) in Table II of Ding *et al.* using the following standard relation for an $M1$ transition $i \rightarrow f$:

$$S^{M1}_{\rm if} = \frac{g_i \lambda^3_{\rm if}}{2.697\,35 \times 10^{13}} A^{M1}_{\rm if}, \qquad (3)$$

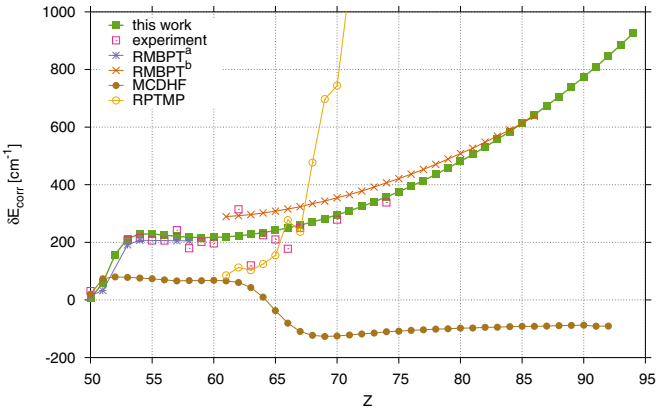

FIG. 5. (Color online) Estimated absolute contributions from core-valence correlation to the $4f\,^2F^o$ fine-structure separation ($\delta E_{\rm corr} = E^{\rm method} - E^{\rm FCV}_{\rm DF}$ where the "method" superscript should be replaced by the corresponding label in the legend) for experiment and other available theory (RMBPT[a] [12], RMBPT[b] [12] (from Ref. [13]), MCDHF [15], and RPTMP [13,14]).

TABLE III. Wavelengths in vacuum ($\lambda_{\rm vac}$), transition rates (A), weighted oscillator strengths (gf), and line strengths (S) of the $4f\,^2F^o_{5/2}$–$^2F^o_{7/2}$ magnetic-dipole ($M1$) transition of Ag-like ions between $Z = 50$ and 94 from the large-scale FCV calculation. Note that the $J = 7/2$ is the lowest level up to and including $Z = 52$; then the two levels cross and and $J = 5/2$ becomes the lower of the two from $Z \geqslant 53$. Numbers in square brackets denotes powers of 10.

Z	$\lambda_{\rm vac}$ (Å)	A (s^{-1})	gf	S
50	1.176[+6]	9.463[−6]	1.178[−8]	3.428
51	7.378[+5]	3.837[−5]	1.879[−8]	3.428
52	2.459[+6]	1.036[−6]	5.638[−9]	3.428
53	4.870[+5]	1.000[−4]	2.846[−8]	3.428
54	1.774[+5]	2.070[−3]	7.814[−8]	3.428
55	9.902[+4]	1.190[−2]	1.400[−7]	3.427
56	6.514[+4]	4.180[−2]	2.127[−7]	3.427
57	4.676[+4]	1.130[−1]	2.963[−7]	3.426
58	3.543[+4]	2.598[−1]	3.910[−7]	3.426
59	2.784[+4]	5.350[−1]	4.975[−7]	3.425
60	2.247[+4]	1.018[+0]	6.164[−7]	3.425
61	1.850[+4]	1.824[+0]	7.486[−7]	3.425
62	1.547[+4]	3.117[+0]	8.949[−7]	3.424
63	1.311[+4]	5.124[+0]	1.056[−6]	3.424
64	1.123[+4]	8.161[+0]	1.233[−6]	3.423
65	9.698[+3]	1.265[+1]	1.427[−6]	3.423
66	8.444[+3]	1.916[+1]	1.639[−6]	3.422
67	7.402[+3]	2.845[+1]	1.869[−6]	3.422
68	6.528[+3]	4.148[+1]	2.120[−6]	3.421
69	5.787[+3]	5.952[+1]	2.391[−6]	3.421
70	5.155[+3]	8.420[+1]	2.683[−6]	3.420
71	4.612[+3]	1.176[+2]	2.999[−6]	3.420
72	4.142[+3]	1.623[+2]	3.339[−6]	3.419
73	3.733[+3]	2.216[+2]	3.703[−6]	3.419
74	3.376[+3]	2.995[+2]	4.094[−6]	3.418
75	3.063[+3]	4.011[+2]	4.513[−6]	3.418
76	2.786[+3]	5.326[+2]	4.960[−6]	3.417
77	2.542[+3]	7.017[+2]	5.436[−6]	3.417
78	2.324[+3]	9.175[+2]	5.944[−6]	3.416
79	2.130[+3]	1.191[+3]	6.484[−6]	3.415
80	1.957[+3]	1.537[+3]	7.057[−6]	3.415
81	1.801[+3]	1.970[+3]	7.666[−6]	3.414
82	1.661[+3]	2.511[+3]	8.310[−6]	3.414
83	1.535[+3]	3.182[+3]	8.992[−6]	3.413
84	1.421[+3]	4.012[+3]	9.712[−6]	3.412
85	1.317[+3]	5.032[+3]	1.047[−5]	3.412
86	1.223[+3]	6.283[+3]	1.128[−5]	3.411
87	1.138[+3]	7.807[+3]	1.212[−5]	3.410
88	1.060[+3]	9.660[+3]	1.301[−5]	3.410
89	9.884[+2]	1.190[+4]	1.395[−5]	3.409
90	9.231[+2]	1.461[+4]	1.493[−5]	3.408
91	8.632[+2]	1.786[+4]	1.596[−5]	3.407
92	8.082[+2]	2.176[+4]	1.705[−5]	3.407
93	7.576[+2]	2.641[+4]	1.818[−5]	3.406
94	7.110[+2]	3.195[+4]	1.937[−5]	3.405

where g_i is the degeneracy of the initial state, $\lambda_{\rm if}$ the transition wavelength in units of Å, and $A^{M1}_{\rm if}$ the $M1$ transition rate in s^{-1}. Comparing the obtained line strength values with ours (Table III) it is clear that the difference is less than or around 0.1% for most members of the sequence. The comparison

does, however, reveal unexplainable trend breaking leaps in the line strength of Ding *et al.* for ions with $Z \leqslant 54$. This comparison further strengthens the analysis that an inaccurate energy separation is the underlying reason for the transition rate discrepancy of the two calculations.

IV. CONCLUSIONS

In this work we have presented a systematic MCDHF study of the $4f\,^2F^o$ fine-structure separation and the magnetic-dipole transition for Ag-like ions with nuclear charges $Z = 50 - 94$. Special attention has been paid to core-valence effects with deep core subshells and it was shown that core-valence correlation with $3d$, rather than $4d$, is the dominant contributor for intermediate and highly charged ions. The underlying reason for this could be an interesting case for further studies. Our large-scale MCDHF calculations include correlation effects from Coulomb- and (frequency-independent) Breit interaction, as well as corrections due to dominant QED effects. The accuracy of the $^2F^o$ fine-structure separation is carefully analyzed through systematic studies of convergence trends as the active set of virtual Dirac orbitals, used to construct the many-body basis, is increased. This is augmented by studies of the smoothness of different properties along the isoelectronic sequence. Furthermore, a good agreement with experiments, of which some are very recent EBIT measurements [5,6], and other reliable theoretical results, finally leads us to conclude that our method provides accurate data for the $^2F^o$ levels of Ag-like ions. Transition rates, weighted oscillator strengths, and line strengths of the magnetic-dipole transition between these two fine-structure levels have been calculated and tabulated. These data should be accurate since the $M1$ operator is not dependent on the radial part of the wave functions, and the transitions energies are accurately predicted.

ACKNOWLEDGMENTS

This work was supported by the National Natural Science Foundation of China under Project No. 11074049 and by the Shanghai Leading Academic Discipline Project B107. We also gratefully acknowledge support from the Swedish Research Council (Vetenskapsrådet) and the Swedish Institute under the Visby-programme. J.G. and W.L. especially thank the Nordic Centre at Fudan University for supporting an exchange between Lund and Fudan. Finally, the authors thank Gordon Berry, Jörgen Ekman, and Per Jönsson for valuable discussions.

[1] B. Edlén, Z. Astrophys. **22**, 30 (1943).
[2] B. Edlén, Mon. Not. R. Astron. Soc. **105**, 323 (1945).
[3] S. Suckewer and E. Hinnov, Phys. Rev. Lett. **41**, 756 (1978).
[4] J. Sugar and V. Kaufman, Phys. Rev. A **21**, 2096 (1980).
[5] Z. Fei, R. Zhao, Z. Shi, J. Xiao, M. Qiu, J. Grumer, M. Andersson, T. Brage, R. Hutton, and Y. Zou, Phys. Rev. A **86**, 062501 (2012).
[6] R. Zhao (private communication, 2014).
[7] S. Morita, C. F. Dong, M. Goto, D. Kato, I. Murakami, H. A. Sakaue, M. Hasuo, F. Koike, N. Nakamura, T. Oishi *et al.*, AIP Conf. Proc. **1545**, 143 (2013).
[8] I. Martinson and C. Jupén, J. Chin. Chem. Soc. **48**, 469 (2001).
[9] A. Lapierre, U. Jentschura, J. C. López-Urrutia, J. Braun, G. Brenner, H. Bruhns, D. Fischer, A. G. Martínez, Z. Harman, W. Johnson *et al.*, Phys. Rev. Lett. **95**, 183001 (2005).
[10] E. Träbert, P. Beiersdorfer, and G. V. Brown, Phys. Rev. Lett. **98**, 263001 (2007).
[11] Y. Ralchenko, J. Phys. B **40**, F175 (2007).
[12] U. I. Safronova, I. M. Savukov, M. S. Safronova, and W. R. Johnson, Phys. Rev. A **68**, 062505 (2003).
[13] E. Ivanova, At. Data Nucl. Data Tables **97**, 1 (2011).
[14] E. Ivanova, At. Data Nucl. Data Tables **95**, 786 (2009).
[15] X.-B. Ding, F. Koike, I. Murakami, D. Kato, H. A. Sakaue, C.-Z. Dong, and N. Nakamura, J. Phys. B. **45**, 035003 (2012).
[16] P. Jönsson, G. Gaigalas, J. Bieroń, C. F. Fischer, and I. P. Grant, Comput. Phys. Commun. **184**, 2197 (2013).
[17] K. Dyall, I. Grant, C. Johnson, F. Parpia, and E. Plummer, Comput. Physics Commun. **55**, 425 (1989).
[18] F. A. Parpia, C. F. Fischer, and I. P. Grant, Comput. Phys. Commun. **94**, 249 (1996).
[19] I. P. Grant, *Relativistic Quantum Theory of Atoms and Molecules: Theory and Computation (Springer Series on Atomic, Optical, and Plasma Physics)* (Springer-Verlag, New York, 2006).
[20] C. Froese Fischer, T. Brage, and P. Jönsson, *Computational Atomic Structure: An MCHF approach* (Institute of Physics, Bristol, 1997).
[21] L. W. Fullerton and G. A. Rinker, Phys. Rev. A **13**, 1283 (1976).
[22] P. J. Mohr, At. Data Nucl. Data Tables **29**, 453 (1983).
[23] C. E. Moore, in *Nat. Stand. Ref. Data Ser. 35*, Vol. III, 245 pp. (Nat. Bur. Stand., U.S., 1971) (Reprint of NBS Circ. 467, Vol. III, 1958).
[24] A. Kramida, Y. Ralchenko, J. Reader, and NIST ASD Team, NIST Atomic Spectra Database (ver. 5.0)[http://www.nist.gov/pml/data/asd.cfm] (2012).
[25] V. Kaufman and J. Sugar, Phys. Scr. **24**, 738 (1981).
[26] M. O. Larsson, A. M. Gonzalez, R. Hallin, F. Heijkensköld, R. Hutton, A. Langereis, B. Nyström, G. O'Sullivan, and A. Wännström, Phys. Scr. **51**, 69 (1995).
[27] A. Tauheed and Y. Joshi, Phys. Scr. **72**, 385 (2005).
[28] S. Churilov and Y. Joshi, Phys. Scr. **62**, 282 (2000).
[29] J. Sugar and V. Kaufman, Phys. Scr. **24**, 742 (1981).